

LETTER TO THE EDITOR

Restarted activity in the 3C 328 radio galaxy

A. Marecki

Institute of Astronomy, Nicolaus Copernicus University, Faculty of Physics, Astronomy and Informatics, Grudziądzka 5,
87-100 Toruń, Poland
e-mail: amr@astro.uni.torun.pl

Received 8 April 2021 / Accepted 20 April 2021

ABSTRACT

As a rule, both lobes of Fanaroff-Riley (FR) type-II radio sources are terminated with hotspots, but the 3C 328 radio galaxy is a specimen of an FR II-like object with a hotspot in only one lobe. A conceivable reason for such asymmetry is that the nucleus of 3C 328 was temporarily inactive. There was no energy transfer from it to the lobes during the period of quiescence, and so they began to fade out. However, under the assumption that the axis connecting the two lobes makes an appreciable angle with the sky plane, and hence one is considerably farther from the observer than the other, the lobes are observed at two distinct stages of evolution due to the light-travel lag. While the far-side lobe is still perceived as being of the FR II type with a hotspot, decay of the near-side lobe is already apparent. No jets are visible in the VLA images, but the VLBA observations of the inverted-spectrum core component of 3C 328 have revealed that it has a jet of a sub-arcsecond length pointing towards the lobe that shows evidence of decay. Since the jet always points to the near side, its observed orientation is in line with the scenario proposed here. The presence of the jet supports the inference that the nucleus of 3C 328 is currently active; however, given the fact that the jet is short (~ 200 pc in projection), the activity must have restarted very recently. The lower and upper limits of the quiescent period length have been calculated.

Key words. galaxies: active — galaxies: nuclei — galaxies: jets — galaxies: individual: 3C 328 — radio continuum: galaxies

1. Introduction

The intermittent nature of active galactic nuclei (AGNs) can manifest itself in a number of ways. A direct observable indication of the cessation and subsequent restart of activity in a radio-loud AGN takes the form of a double-double radio source (DDRS; Schoenmakers et al. 2000) consisting of two co-linear pairs of radio lobes (see Saikia & Jamrozy 2009 for a review and e.g. Marecki et al. 2021 for references to the latest papers on DDRSs). If the inner lobes resulting from the second active phase of a DDRS had been created only recently, their separation could have been too small to render them as a double in the image depicting the overall structure of the source. It follows that as long as the putative ‘core’ is not resolved, the true nature of this kind of object remains unknown. B 0818+214 is a good example demonstrating such a case. Only MERLIN and the EVN observations revealed that its central component, which is straddled by a pair of large-scale lobes as seen in the Faint Images of the Radio Sky at Twenty centimeters (FIRST) survey (Becker et al. 1995), is actually the inner double that is two orders of magnitude more compact than the co-linear outer double (Marecki & Szablewski 2009). Therefore, although seemingly a core-dominant triple (CDT), B 0818+214 is also a DDRS.

However, a conjecture that every CDT is a concealed DDRS, such as is the case of B 0818+214, would be misguided. Marecki & Swoboda (2011, hereafter Paper I) studied three quasi-stellar objects (QSOs) that are CDTs whose lobes are asymmetric: While a hotspot is present in one of the two lobes of each of these QSOs, the other is diffuse and lacks a hotspot. According to the authors, the cause of this phenomenon is as follows. The activity of the nuclei in those objects has ceased, and hence the energy supply to the lobes has been cut off. As a con-

sequence, as the lobes weaken and become diffuse, the hotspots vanish. If the axis of a double-lobed radio source lies far from the sky plane, which is the case for QSOs (Barthel 1989), then the perceived epoch of the far-side lobe is considerably earlier than the perceived epoch of the near-side lobe due to the light-travel time (Gopal-Krishna et al. 1996). For large-scale sources, the difference between those epochs may be of the order of at least 10^5 years. Since the lifetimes of the hotspots are 7×10^4 yr (Kaiser et al. 2000), such light-travel time is sufficient for the hotspot of the near-side lobe to disappear while the hotspot of the far-side lobe is still observable. This kind of the lobe asymmetry can thus be regarded as a signature of a recent termination of activity. Indeed, the EVN observations reported in Paper I show that the cores of those CDTs are typical for radio-quiet AGNs (Ulvestad et al. 2005).

By no means is the lopsidedness of the lobes highlighted above limited to QSOs. It is just as likely to take place in a radio galaxy, unless such a galaxy lies close to the sky plane, provided that its lobe-to-lobe span is sufficiently large for the aforementioned time lag to become significant. For example, the morphology of the 3C 16 radio galaxy can be explained within the framework of that scenario. It is asymmetric in the same manner: Whereas the south-western lobe is of a Fanaroff-Riley (FR) type II (Fanaroff & Riley 1974), the north-eastern one is devoid of a hotspot (see the images in Leahy & Perley 1991, Harvanek & Hardcastle 1998, and Gilbert et al. 2004). The nucleus of 3C 16 is not just radio quiet; given that there is no radio core visible, it is fully radio silent. As the activity has ceased in this object, it could be labelled ‘post-active’.

Post-active objects can, however, revert to the active state. Active galactic nuclei such as J1211+743 (see the image in Pirya et al. 2011) as well as 3C 249.1 and 3C 334 (see the im-

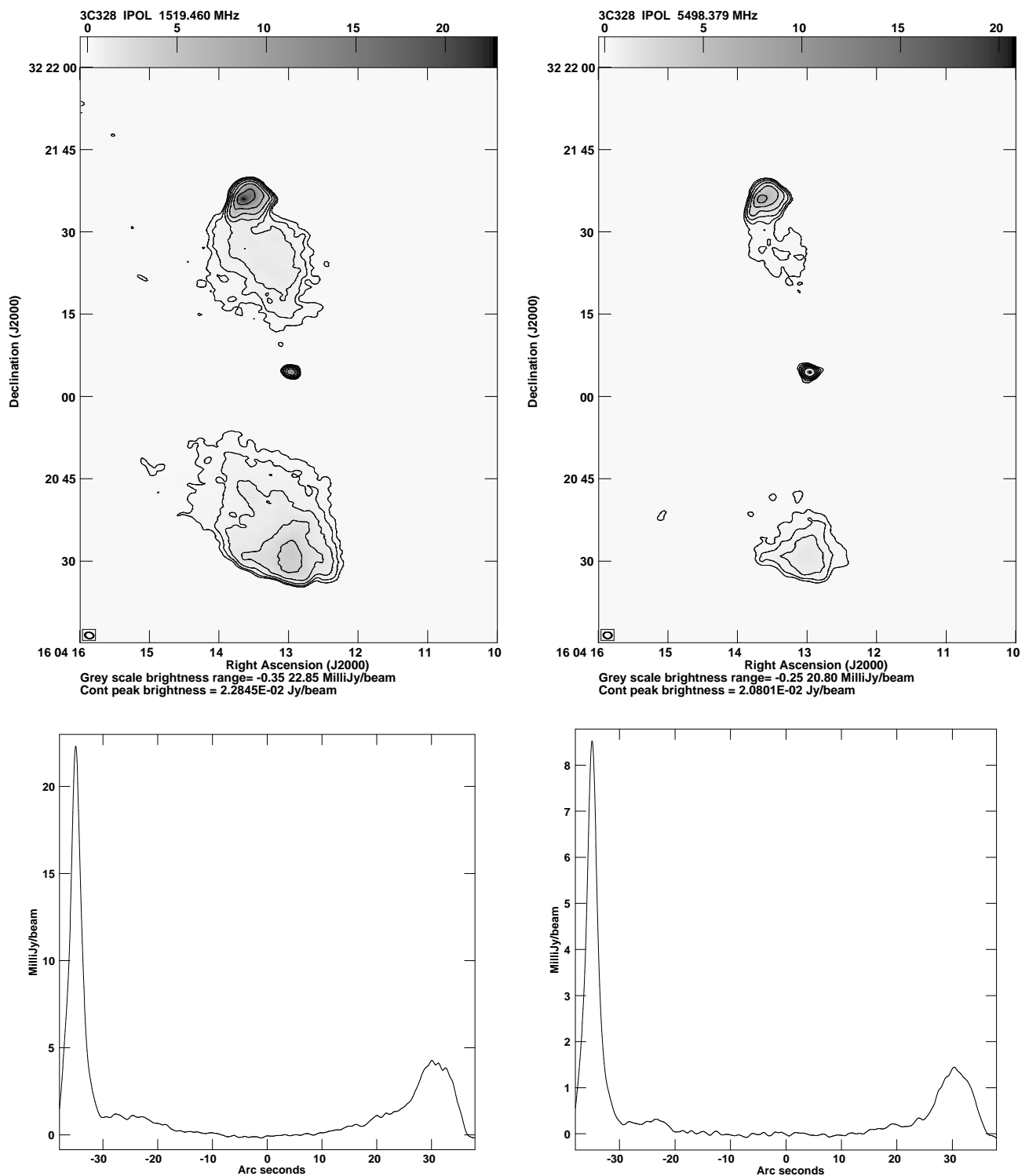


Fig. 1. Outcome of the VLA observations. *Upper panels:* Images of 3C 328 at 1.5 GHz (*left-hand panel*) and at 5.5 GHz (*right-hand panel*). In both images, contours are at 0.2, 0.4, 0.8, 1.6, 3.2, 6.4, 12.8, and 25.6 mJy/beam. *Lower panels:* Slices across the lobes at 1.5 GHz (*left-hand panel*) and at 5.5 GHz (*right-hand panel*). North is on the left-hand side of each plot. The core has been bypassed by both slices.

ages in Gilbert et al. 2004) have restarted. These three AGNs are unique for two reasons. Firstly, they evince the asymmetry of the type described above, and secondly their jets are oriented towards the lobe with no hotspot. As posited by the light-travel-time-based scenario, the lobe showing evidence of decay must be on the near side. Since the jet always signposts the near side, such an orientation of the jet supports that model. Detailed stud-

ies of these three sources are presented in Marecki (2012a, hereafter Paper II), where the model was introduced and applied to J1211+743, as well as in Marecki (2012b, hereafter Paper III), where it was applied to 3C 249.1 and 3C 334.

Radio galaxy 3C 328 (B2 1602+324) is also a source that has one FR II-type lobe and whose other lobe has no hotspot (see the VLA image at 1465 MHz in Machalski & Condon 1983).

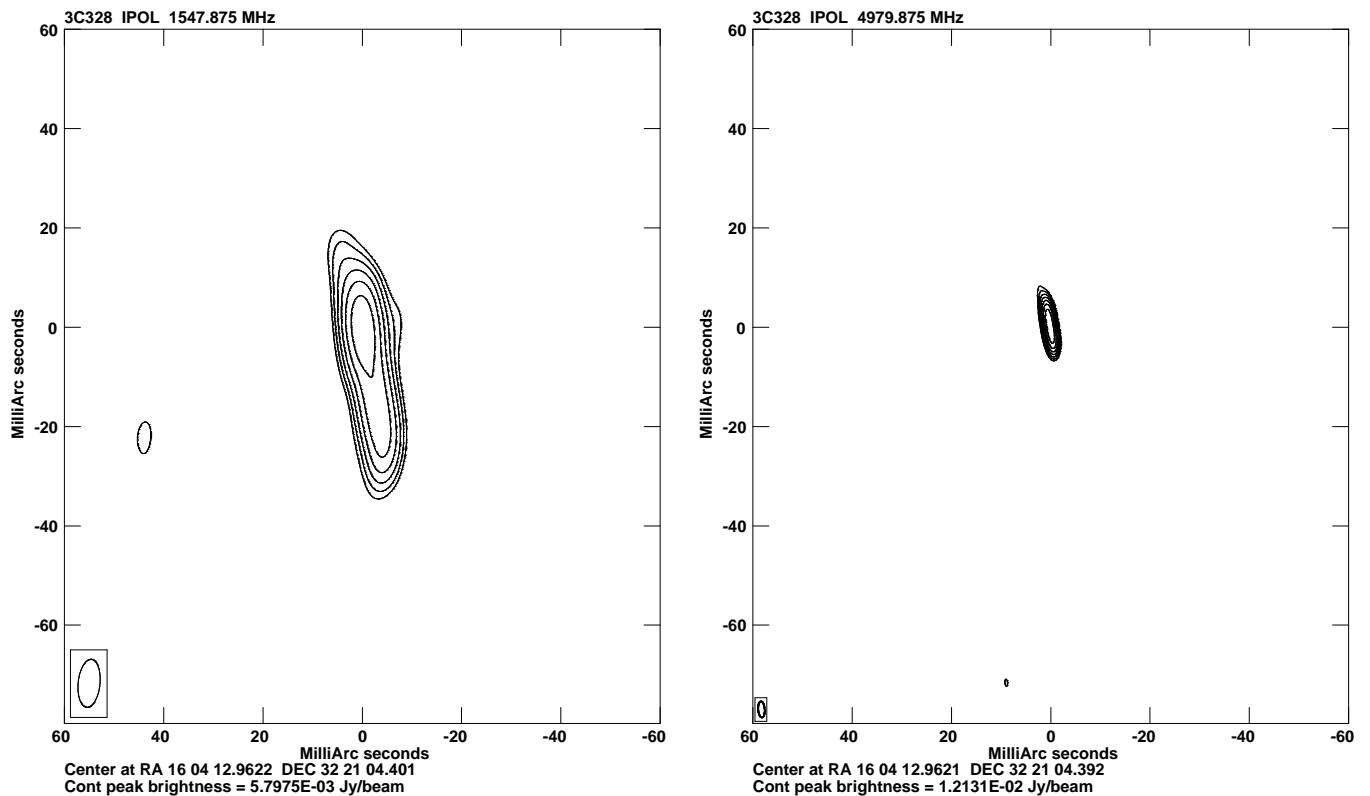


Fig. 2. VLBA images of 3C 328 at 1.5 GHz (*left-hand panel*) and at 5 GHz (*right-hand panel*). In both images, contours are at 0.1, 0.2, 0.4, 0.8, 1.6, 3.2, 6.4, and 12.8 mJy/beam.

Moreover, there is a point-like core at the centre, so the morphology of 3C 328 very much resembles that of the QSOs from Paper I despite the fact that it is not a QSO but rather a galaxy. Whether it has a switched-off nucleus like those QSOs or is restarted is not known. To investigate the current state of activity of the nucleus of 3C 328, the VLA and VLBA observations have been carried out, and their outcome is reported here. The following values of cosmological parameters are used in this Letter: $H_0 = 67.4 \text{ km s}^{-1} \text{ Mpc}^{-1}$, $\Omega_M = 0.315$, and $\Omega_\Lambda = 0.685$ (Planck Collaboration VI 2020); hence, for the redshift of 3C 328, $z = 0.45243$, 1 arcsec of the angular size translates to 5.971 kpc.

2. Observations

The VLA observations were performed in two configurations: ‘B’ at two 1024-megahertz-wide frequency bands centred at 5 and 6 GHz on 11 March 2019, and ‘A’ at two 512-megahertz-wide frequency bands centred at 1264 and 1776 MHz on 9 October 2019. In each of those two runs, 3C 328 was observed for 10 min. J1606+3124 was used as a phase calibrator. Continuum data reduction was carried out using the VLA CASA calibration pipeline. The 1.5 GHz images were generated with Briggs weighting, which yields a good trade-off between resolution and sensitivity. The same weighting was initially used for the 5.5 GHz data, but the diffuse features of the object were poorly rendered in the image. Therefore, the natural weighting that yields the highest signal-to-noise ratio at the cost of a poorer angular resolution was eventually applied. After adopting this scheme, the restoring beam sizes at both frequencies were very similar: $1''.59 \times 1''.12$ at 1.5 GHz and $1''.52 \times 1''.18$ at 5.5 GHz.

The VLBA observations were performed on 8 June 2013 at two 256-megahertz-wide frequency bands centred at 1552 MHz and 4980 MHz. In each of these two bands, 3C 328 was observed for 100 min. The restoring beam sizes were 9.70×4.40 mas at 1.5 GHz and 3.29×1.30 mas at 5 GHz.

Table 1. Flux densities of the components of 3C 328.

Frequency [MHz]	Flux densities [mJy]			
	Northern lobe	Southern lobe	Northern hotspot	Core
1519	264	242	107	12.2
5498	71	51	34	21.4

3. Results

The VLA images resulting from the observations mentioned in Sect. 2 are presented in the upper panels of Fig. 1. While the hotspot is present in the northern lobe, the absence of a hotspot in the southern lobe is conspicuous, particularly at 5.5 GHz (upper right-hand panel of Fig. 1). The dominance of the only hotspot is highlighted by the slices running across both lobes but bypassing the core (lower panels of Fig. 1). The flux densities of the lobes measured with TVSTAT AIPS Utility as well as those of the core component and the hotspot of the northern lobe – both measured with JMFIT AIPS Task – are displayed in Table 1. A compelling trait of 3C 328 revealed by the data shown there is that the core is stronger at 5.5 GHz than at 1.5 GHz, which means that it has an inverted spectrum ($\alpha_{1.5}^{5.5} = 0.44$, $S \propto \nu^\alpha$) between these two frequencies. This feature has been confirmed by the measurement of the flux density at the intermediate frequency of 3 GHz.

Table 2. Lower and upper limits to the length of the quiescent period.

θ [$^\circ$]	t_q^{\min} [Myr]			t_q^{\max} [Myr]		
	$\beta_{\text{jet}}=0.8$	0.9	1.0	$\beta_{\text{jet}}=0.8$	0.9	1.0
45	0.65	0.50	0.38	1.91	1.78	1.67
50	0.67	0.53	0.42	1.71	1.58	1.48
60	0.72	0.60	0.50	1.39	1.28	1.20
70	0.80	0.69	0.60	1.17	1.07	0.99
80	0.89	0.79	0.70	1.00	0.90	0.82

To this end, the image of 3C 328 was extracted from the *VLA Sky Survey* (VLASS)¹ for Epoch 2.1 with the CIRADA cutout service², and the flux density of the core was measured with JMFIT. It amounts to 15.9 mJy, and the following values of the spectral indices were obtained: $\alpha_{1.5}^{3.0} = 0.39$ and $\alpha_{3.0}^{5.5} = 0.49$. The observations that led to the flux-density measurements at those three frequencies were carried out in similar epochs, and therefore the impact of the potential long-term variability of the core of 3C 328 should not be significant. It seems that such a variability does indeed take place there. According to the FIRST survey, the 1.4 GHz flux density of the core of 3C 328 as observed about two decades earlier amounts to 17.4 mJy. It appears then that the flux density of the core, at least at frequencies around 1.5 GHz (see Table 1), has been on the decline ever since.

Based on the outcome of the two-frequency VLA observations, the inverted-spectrum core must be self-absorbed, and hence very compact. Its VLBA images resulting from the observations mentioned in Sect. 2 are shown in Fig. 2. At 5 GHz, the core of 3C 328 is point-like, while at 1.5 GHz it has an additional feature elongated southwards. As the same phase reference was used throughout those observations (J1606+3124), the absolute positions of the source at both frequencies were preserved. The core visible at 5 GHz is co-incident with the brightest part of the source in the 1.5 GHz image, and thus this image depicts a core-jet structure where the jet points to the southern lobe. This means that, apart from the lobe asymmetry, there is another similarity that 3C 328 shares with J1211+743, 3C 249.1, and 3C 334: All these AGNs have jets that point towards the lobe that is devoid of a hotspot. This raises the question of whether the light-travel-time-based model elaborated on in Paper II for J1211+743 and then used to interpret 3C 249.1 and 3C 334 in Paper III could also be applied to 3C 328. To find that out, one has to perform a quantitative test using that model since it imposes tight constraints on both the lower and upper limits of the length of the period of quiescence, t_q .

The projected angular far-side and near-side arm lengths of 3C 328 (35''6 and 38''8) respectively translate to 212 kpc and 232 kpc of the projected linear size, whereas the projected angular size of the jet (0''035) translates to 209 pc of the projected linear size. For these linear sizes, the lower (t_q^{\min}) and upper (t_q^{\max}) limits of t_q were calculated using Eqs. (2) and (4) of Paper II for $\beta_{\text{adv}} = 0.35$, three values of β_{jet} (0.8, 0.9, and 1), and five values of the angle between the line of sight and the AGN axis θ . Since 3C 328 is a galaxy and not a QSO, only the values $\theta \geq 45^\circ$ are applicable to it (Barthel 1989). The results are shown in Table 2. Due to the small size of the jet in 3C 328, the calculated limits are almost independent from the adopted value of β_{adv} . The definitions of β_{jet} and β_{adv} are provided in Paper II.

4. Conclusion

Taking into account that for at least two restarted AGNs – 3C 293 (Machalski et al. 2016) and J1835+6204 (Konar et al. 2012) – the values of t_q also stay within the limits shown in Table 2, it is plausible that the above limits for t_q may be valid for 3C 328, and as such the light-travel-time-based scenario can be used to explain its nature. It follows that the activity of 3C 328 has restarted and, given the minute size of its jet, that this happened recently. The images presented here are thus a record of two subsequent transitions in the nucleus of 3C 328: 1) from the active to the inactive state, which is expressed by the asymmetry of the lobes, and 2) back to the active state, represented by the sub-kiloparsec-scale jet. The bottom line is that, in terms of the stage of the recurrent activity, the eight asymmetric objects mentioned in this Letter can be arranged in chronological order:

1. The objects studied in Papers II and III restarted a relatively long time ago, which has allowed their jets to attain large sizes.
2. Galaxy 3C 328 has recently restarted after a period of quiescence.
3. Galaxy 3C 16 is quiescent.
4. The objects described in Paper I have just switched off.

Acknowledgements. The National Radio Astronomy Observatory is a facility of the National Science Foundation operated under cooperative agreement by Associated Universities, Inc. This research has made use of the CIRADA cutout service at URL cutouts.cirada.ca, operated by the Canadian Initiative for Radio Astronomy Data Analysis (CIRADA). CIRADA is funded by a grant from the Canada Foundation for Innovation 2017 Innovation Fund (Project 35999), as well as by the Provinces of Ontario, British Columbia, Alberta, Manitoba and Quebec, in collaboration with the National Research Council of Canada, the US National Radio Astronomy Observatory and Australia's Commonwealth Scientific and Industrial Research Organisation. This research has made use of the NASA/IPAC Extragalactic Database (NED), which is funded by the National Aeronautics and Space Administration and operated by the California Institute of Technology. I am grateful to Marek Jamrozny for critical reading of the draft of this Letter and a number of suggestions that improved it.

References

- Barthel, P. D. 1989, *ApJ*, 336, 606
Becker, R. H., White, R. L., & Helfand, D. J. 1995, *ApJ*, 450, 559
Fanaroff, B. L., & Riley, J. M. 1974, *MNRAS*, 167, 31P
Gilbert, G. M., Riley, J. M., Hardcastle, M. J., et al. 2004, *MNRAS*, 351, 845
Gopal-Krishna, Wiita, P. J., & Hooda, J. S. 1996, *A&A*, 316, L13
Harvanek, M., & Hardcastle, M. J. 1998, *ApJS*, 119, 25
Kaiser, C. R., Schoenmakers, A. P., & Röttgering, H. J. A. 2000, *MNRAS*, 315, 381
Konar, C., Hardcastle, M. J., Jamrozny, M., Croston, J. H., & Nandi, S. 2012, *MNRAS*, 424, 1061
Lacy, M., Baum, S. A., Chandler, C. J., et al. 2020, *PASP*, 132, 035001
Leahy, J. P., & Perley, R. A. 1991, *AJ*, 102, 537
Machalski, J., & Condon, J. J. 1983, *AJ*, 88, 143
Machalski, J., Jamrozny, M., Stawarz, Ł., & Weżgowiec, M. 2016, *A&A*, 595, A46
Marecki, A. 2012a, *A&A*, 544, L2
Marecki, A. 2012b, *A&A*, 545, A132
Marecki, A., & Szablewski, M. 2009, *A&A*, 506, L33
Marecki, A., & Swoboda, B. 2011, *A&A*, 525, A6
Marecki, A., Jamrozny, M., Machalski, J., & Pajdosz-Śmierciak, U. 2021, *MNRAS*, 501, 853
Pirya, A., Nandi, S., Saikia, D. J., Konar, C., & Singh, M. 2011, *Bull. Astron. Soc. India*, 39, 547
Planck Collaboration VI. 2020, *A&A*, 641, A6
Saikia, D. J., & Jamrozny, M. 2009, *Bull. Astron. Soc. India*, 37, 63
Schoenmakers, A. P., de Bruyn, A. G., Röttgering, H. J. A., van der Laan, H., & Kaiser, C. R. 2000, *MNRAS*, 315, 371
Ulvestad, J. S., Antonucci, R. R. J., & Barvainis, R. 2005, *ApJ*, 621, 123

¹ The science case, the observational strategy for VLASS, and the results from early survey observations are presented by Lacy et al. (2020).

² <http://cutouts.cirada.ca/>